Ore Geology Reviews 118 (2020) 103361

Contents lists available at ScienceDirect

Ore Geology Reviews

journal homepage: www.elsevier.com/locate/oregeorev

Geochemistry of magnetite from the giant Paleoproterozoic Dahongshan Fe-Cu deposit, SW China: Constraints on nature of ore-forming fluids and depositional setting

Yan-Jun Wang[a,b], Wei-Guang Zhu[a,*], Hui-Qing Huang[c], Zhong-Jie Bai[a], Hong Zhong[a,d], Jun-Hua Yao[a], Hong-Peng Fan[a]

[a] State Key Laboratory of Ore Deposit Geochemistry, Institute of Geochemistry, Chinese Academy of Sciences, Guiyang 550081, China
[b] State Key Laboratory of Nuclear Resources and Environment, East China University of Technology, Nanchang, Jiangxi 330013, China
[c] Economic Geology Research Center, College of Science and Engineering, Division of Tropical Environments and Societies, James Cook University, Townsville, QLD 4811, Australia
[d] College of Earth and Planetary Sciences, University of Chinese Academy of Sciences, Beijing 100049, China

ARTICLE INFO

Keywords:
Paleoproterozoic
Magnetite
Trace element
Dahongshan Fe-Cu deposit
Southwestern China

ABSTRACT

The Dahongshan Fe-Cu ore deposit, hosted in the Paleoproterozoic meta-volcanic and meta-sedimentary sequences, is a giant deposit in the Fe-Cu metallogenic province of southwestern China. Two ore types have been identified: (1) massive and disseminated Fe ores hosted dominantly in meta-volcanic rocks and (2) disseminated and banded Fe-Cu ores in meta-sedimentary rocks. Magnetite presents in all orebodies, and is dominant in the Fe ores. Chemistry of magnetite suggest that the fluids for iron mineralization in the Fe and Fe-Cu orebodies are likely chemically similar and cogenetic. Minor sulfides (e.g., molybdenite) occur at the end of iron mineralization stage, indicating the gradually decrease in oxygen fugacity for the mineralizing fluids with magnetite precipitation. Along with evolution, mineralizing fluids generate magnetite with depletions in Cr, Ni, Ga and V, but enrichments in Mn, Sn and Co, which are primarily reflective of the temperature decrease of fluids.

We have discovered some magnetite grains that are extremely rich in V (~10000 ppm), but low in Ti and Cr. Geochemical patterns suggest that they were formed by fluids similar to those of ordinary ores. Available knowledge about the unique high-V magnetite indicates highly-reduced marine environments for its generation. Ore bulk REE patterns showing remarkable positive Eu anomalies and absence of obvious Ce anomalies suggest a BIF-like marine environment, consistent with the morphology of both Fe and Fe-Cu orebodies. Our results provide independent evidence for submarine environment in the formation of the giant Precambrian stratiform Fe(-Cu) ore deposit.

1. Introduction

There is a significant Fe-Cu metallogenic province in the Kangdian region extending from Sichuan Province in the north, through Yunnan Province, to northern Vietnam in the south (Sun et al., 1991; Zhao and Zhou, 2011; Chen and Zhou, 2012; Zhou et al., 2014). Geological exploration indicates that at least 600 Mt iron and 5 Mt copper have been preserved in this metallogenic province (Qian and Shen 1990; Zhou et al., 2014). These Fe-Cu deposits are primarily hosted in Paleoproterozoic meta-volcanic and meta-sedimentary sequences, but are commonly crosscut by mafic intrusions (Qian and Shen, 1990; Kou et al., 2017; Zhao et al., 2017). Geochronological studies reveal that these deposits have been overprinted by hydrothermal events associated with multiple regional tectonic events during 1.7–0.8 Ga (Li et al., 2003; Zhao and Zhou 2011; Chen and Zhou 2012; Fan et al., 2013; Ye et al., 2013; Zhao et al., 2013, 2017; Zhou et al., 2014; Li and Zhou, 2015; Zhu et al., 2017; Wang et al., 2019), coinciding with formation and breakup of supercontinents Nuna/Columbia and Rodinia (Zhou et al., 2014). However, it is still controversial about the genesis of Fe-Cu deposits in the region. The mainstream volcanic-hosted model suggests that these deposits formed by processes like those of VHMS (volcanic-hosted massive sulfide deposits) or SEDEX (sedimentary exhalative deposits), which emphasizes the significance of submarine volcanic activities (Qian and Shen, 1990; Sun et al., 1991; Yang et al., 2004; Wu et al., 2008; Ye et al., 2013; Zhang et al., 2014a,b; Kou et al., 2017). The alternative model, developed on similarities of mineralization type of

* Corresponding author.
E-mail address: zhuweiguang@vip.gyig.ac.cn (W.-G. Zhu).

https://doi.org/10.1016/j.oregeorev.2020.103361
Received 11 July 2018; Received in revised form 3 January 2020; Accepted 22 January 2020
Available online 25 January 2020
0169-1368/

these deposits with the IOCG deposits, supports significant material contributions from magmas that formed regional mafic intrusions (Zhao et al., 2010; Zhao and Zhou 2011; Chen and Zhou 2012; Hou et al., 2015a,b; Zhao et al., 2017). A remarkable feature for the former model is its high dependence on submarine environment for the mineralization, which may be applied to reconcile these two models.

In recent years, there is an increasing use of magnetite in ore deposits for provenance studies as its compositional variation corresponds well with conditions of formation (Dupuis and Beaudoin 2011; Dare et al., 2012, 2014, 2015; Nadoll et al., 2014; Knipping et al., 2015a,b). Together with detailed texture study, chemistry of magnetite grains would provide reliable information about the ore-forming fluids and mineralizing processes (Knipping et al., 2015a,b). Because magnetite dominates the Fe orebodies and presents in the Fe-Cu orebodies of the Dahongshan Fe-Cu deposit, one of the largest Fe-Cu ore deposits in the Kangdian metallogenic province, it would give constraints the nature of the iron mineralizing fluids. In this contribution, we conduct a LA-ICP-MS study on magnetite from the Dahongshan deposit to trace the evolution of mineralizing fluids. Furthermore, we report some unique high-V magnetite, which, combined with whole-rock REE patterns and geological observation on morphology of orebodies, would reveal the ore-forming environment and give insights into the available genetic models for the Dahongshan deposit.

2. Regional geology

The Yangtze Block is one of major Precambrian blocks in China (Fig. 1a). Abundant Proterozoic strata are exposed along the roughly N-S-trending southwestern margin of the Block (Fig. 1b; the so-called Kangdian region). These strata include (1) the Paleoproterozoic Dahongshan Group, Hekou Group, Lower Kunyang Group (Dongchuan Group), and Lower Huili Group, which were deposited at > 1.7–1.5 Ga (Greentree and Li, 2008; Zhao et al., 2010; Chen et al., 2013; Fan et al., 2013; Wang and Zhou, 2014; Geng et al., 2017), (2) the Mesoproterozoic Upper Kunyang and Upper Huili Groups, which were dated at ~1.5–1.0 Ga (Greentree et al., 2006; Zhang et al., 2007; Zhu et al., 2016; Geng et al., 2017), and (3) the early Neoproterozoic Yanbian Group, which were thought to be formed in a continental or oceanic back-arc basin (Li et al., 2006; Zhou et al., 2006).

Both the Dahongshan and Hekou Groups contain volcanic-sedimentary sequences and have experienced low-grade amphibolite facies metamorphism, whereas the Dongchuan Group comprises weakly deformed sedimentary sequences with minor volcanic rocks and has undergone only low-grade greenschist facies metamorphism (Greentree and Li, 2008; Zhou et al., 2014 and references therein). Volcanic layers from the Dahongshan and Hekou Groups have zircon U-Pb ages of 1.68 Ga (Greentree and Li, 2008; Zhao and Zhou, 2011) and 1.7 Ga (Chen et al., 2013), respectively. Zircons from lower and upper tuff layers of the Dongchuan Group yield ages of 1.7 Ga and 1.5 Ga (Sun et al., 2009; Zhao et al., 2010). These three groups were thought to be lateral equivalents in different parts of the area (Zhao et al., 2010). Numerous Proterozoic plutons intruding those groups are ~1.7 Ga and ~1.0 Ga rift-related mafic-felsic rocks and ~860–740 Ma mafic-intermediate-felsic rocks (e.g., Greentree and Li, 2008; Zhao et al., 2010; Zhou et al., 2014; Zhu et al., 2016). Sparse ~1.5 Ga mafic bodies and volcanic counterparts were also reported in the northern part of the region (Sun et al., 2009; Fan et al., 2013).

3. Geology of the Dahongshan Fe-Cu deposit

The Kangdian metallogenic province has minimum reserves of > 600 Mt iron and > 5 Mt copper at early explorations (Qian and Shen, 1990; Sun et al., 1991). Kangdian Fe-Cu deposits are mainly hosted in the Paleoproterozoic Dahongshan, Hekou and Dongchuan Groups. To be specific, the Dahongshan, Dongchuan and Hekou Groups host the Dahongshan, Yinachang and Lala Fe-Cu deposits, respectively, from the south to north of the Kangdian metallogenic province (Fig. 1b). The Dahongshan deposit has a reserve of 458.3 Mt of ore at 41.0% Fe and 1.35 Mt Cu (metal) at 0.78% Cu as the dominant metal types. Moreover, it contains considerable amounts of Au, Ag, Co, Pd and Pt as by products (N9GBYBGMR, 1983).

3.1. The Dahongshan Group

The Dahongshan Group, which hosts the giant Dahongshan Fe-Cu ore deposit, has limited outcrop exposures and is only observed in a narrow triangle area where the NW-trending Red River Zone meets the N-S-trending Luzhijiang Fault Belt (Fig. 1c). From the bottom to top, five formations were identified: the Laochanghe, Mangganghe, Hongshan, Feiweihe, and Potou Formations (Qian and Shen, 1990). The lowermost Laochanghe Formation primarily consists of quartzite with interlaid schist, garnet-muscovite schist and marble. The orebody-hosting Mangganghe Formation is composed of albitized-mable and minor garnet/amphibole/biotite schist and albitized-quartzite (Fig. 2). The overlying Hongshan Formation is divided into the lower thick shallow-colored albitized lava, upper thick dark-colored albitized lava and medium thin garnet-amphibole schist layers (Fig. 2). The Feiweihe Formation is characterized by the massive dolomite marble and carbonaceous slate. The Potou Formation consists of carbonaceous marble, carbonaceous slate and quartzite, and mica schist. All of these strata are overlain by Triassic clastic rocks, mainly sandstone (Fig. 2).

Although Kou et al. (2017) proposed the Dahongshan Group was possibly formed in the mid-Paleoproterozoic, most evidences suggest that the group actually has a late Paleoproterozoic age similar to the Hekou and Dongchuan Groups (Greentree and Li, 2008; Zhao and Zhou, 2011; Yang et al., 2012; Zhou et al., 2014). The basal Laochanghe Formation has zircons from intermediate-felsic rocks yielding zircon ages of 1711 ± 4 Ma and 1686 ± 4 Ma (Yang et al., 2012). Greentree and Li (2008) reported a sensitive high-resolution ion microprobe (SHRIMP) zircon U-Pb age of 1675 ± 8 Ma for similar felsic volcanic rocks, which were also dated at 1681 ± 13 Ma by laser ablation-inductively coupled plasma-mass spectrometry (LA-ICP-MS) (Zhao and Zhou, 2011). All these geochronological data, together with the slightly later intruding mafic rocks (~1.66 Ga, Zhao and Zhou, 2011), constrain the age of deposition of the Dahongshan Group at ~1.7 Ga.

3.2. Mineralization

Meta-volcanic lava, schist and marble from the middle part of the Dahongshan Group, that is the Mangganghe and Hongshan Formations, are the primary wall rocks for Dahongshan orebodies (Fig. 2). Two different orebody groups can be recognized based on the ore mineral assemblages. The iron orebody group is characterized by the combination of dominant magnetite and minor hematite, whereas the iron-copper orebody group contains magnetite, sulfides (mainly chalcopyrite, pyrite and minor bornite) and no hematite (Fig. 3). The Fe orebody group primarily includes orebodies No. II and IV, which are hosted in the lower and upper meta-volcanic rocks of Hongshan Formation, respectively. Much smaller Fe orebody No. V also develops at the top of Hongshan Formation. The Fe-Cu orebody group is mainly composed of orebodies No. I and III, which preferentially occur in the meta-sedimentary rocks of Mangganghe and Hongshan Formation, respectively. All orebodies, except the orebody No. V, are roughly congruent with their country stratification and, as well as these strata, are crosscut by numerous mafic intrusions. The orebody V is irregular-shaped and roughly develops in the contact zones of postdated dolerites and country rocks (Qian and Shen, 1990; Zhao et al., 2017). Given the geochronological data of the Dahongshan Group and mafic intrusions, the best estimate age for the Dahongshan deposit is at 1.66–1.7 Ga. Post-ore modification events are recorded in pyrite from overprinting sulfide veins and molybdenite with Re-Os ages of ~1026 Ma and ~830 Ma, which are coeval with late Mesoproterozoic magmatism and

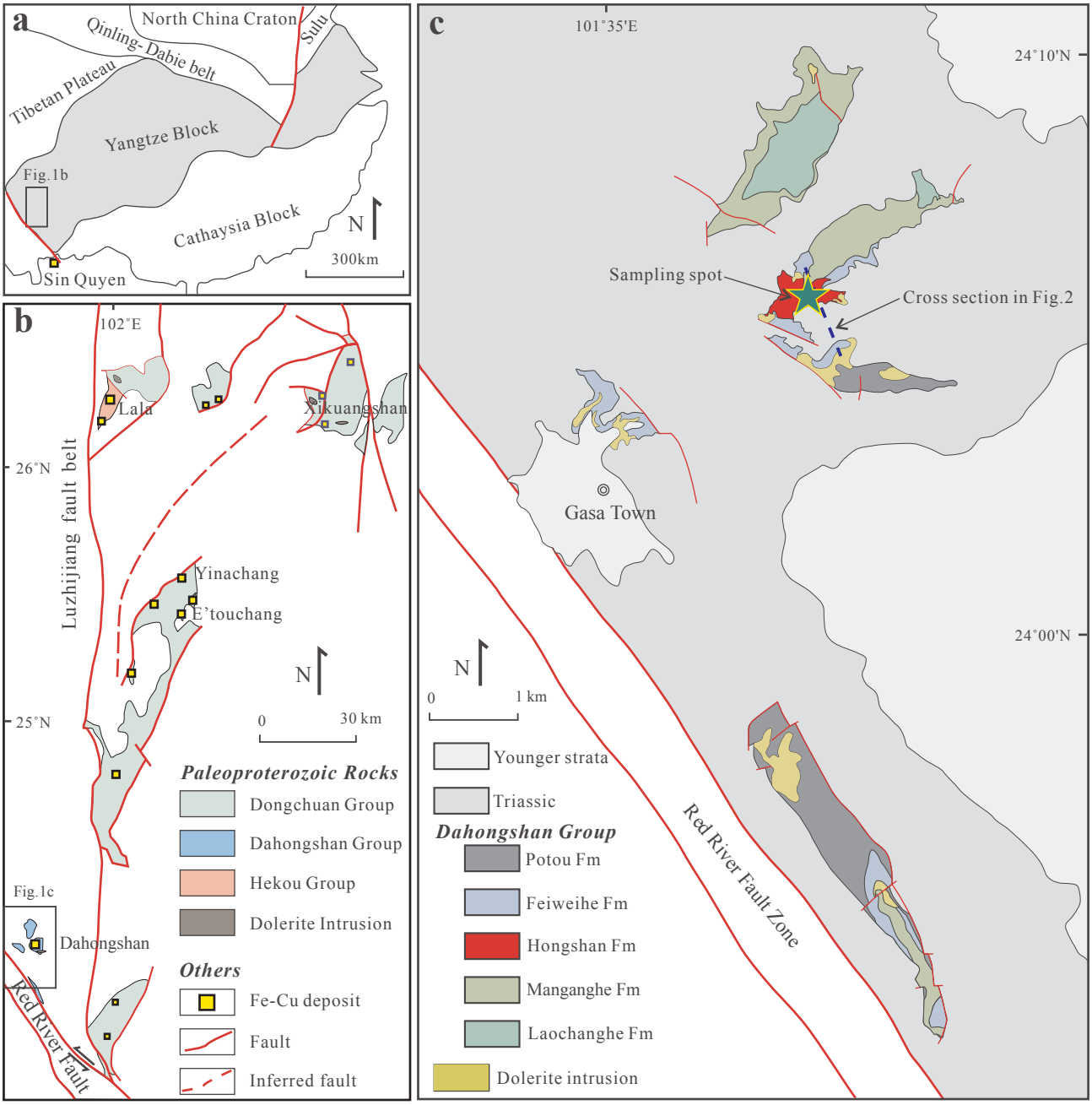

Fig. 1. (a) Schematic map showing the tectonic framework of SW China and Sin Quyen deposit in the northern Vietnam; (b) Schematic geologic map showing distribution of Paleoproterozoic Groups and related Fe-Cu deposits in SW China; (c) Schematic geologic map showing the location of the Dahongshan district (modified after Zhou et al., 2014; Zhao et al., 2017). Dashed line represents the cross section shown in Fig. 2a.

Neoproterozoic metamorphism in the region, respectively (Zhao et al., 2017).

Based on examinations in this study and previous results (Fig. 4; Qian and Shen, 1990; Zhao et al., 2017), the paragenetic sequence of the Dahongshan deposit can be divided into four stages (Fig. 5). Stage I sodic alteration is characterized by pervasive albite and minor scapolite and actinolite. It was followed by stage II iron mineralization with abundant magnetite accompanied with apatite, siderite, ankerite, tourmaline, chlorite, quartz and local K-rich minerals (e.g., K-feldspar and sericite). Minor molybdenite also occurs at the end of this stage. Magnetite dominates stage II and has martitization along its margin in massive iron orebodies. Stage III sulfide stage is associated with potassic-carbonate alteration assemblage, represented by chlorite, sericite, biotite, K-feldspar and ankerite. This stage has abundant chalcopyrite with minor bornite. Pyrite occurs in both stage II and III. After the major ore-forming event, the deposit has suffered from remobilization and overprinting during regional Meso-Neoproterozoic tectonothermal events.

High-V ores were discovered in this study. As shown in Fig. 4a-1, a-2, high-V ores are dominated by magnetite grains, which are spatially closely associated with apatite, ankerite and quartz. Minor chlorite, siderite and ilmenite also occur in these ores. Some tiny quartz inclusions were observed in magnetite grains. By contrast, magnetite grains in ordinary ores (Fig. 4b–d) from the same orebody have roughly equigranular texture similar to that of high-V ores. Gangue minerals in ordinary ores are mainly quartz and ankerite with minor chlorite, biotite, apatite, albite and ilmenite. Inclusions of quartz and albite also occur in the core of magnetite grains. No significant difference between

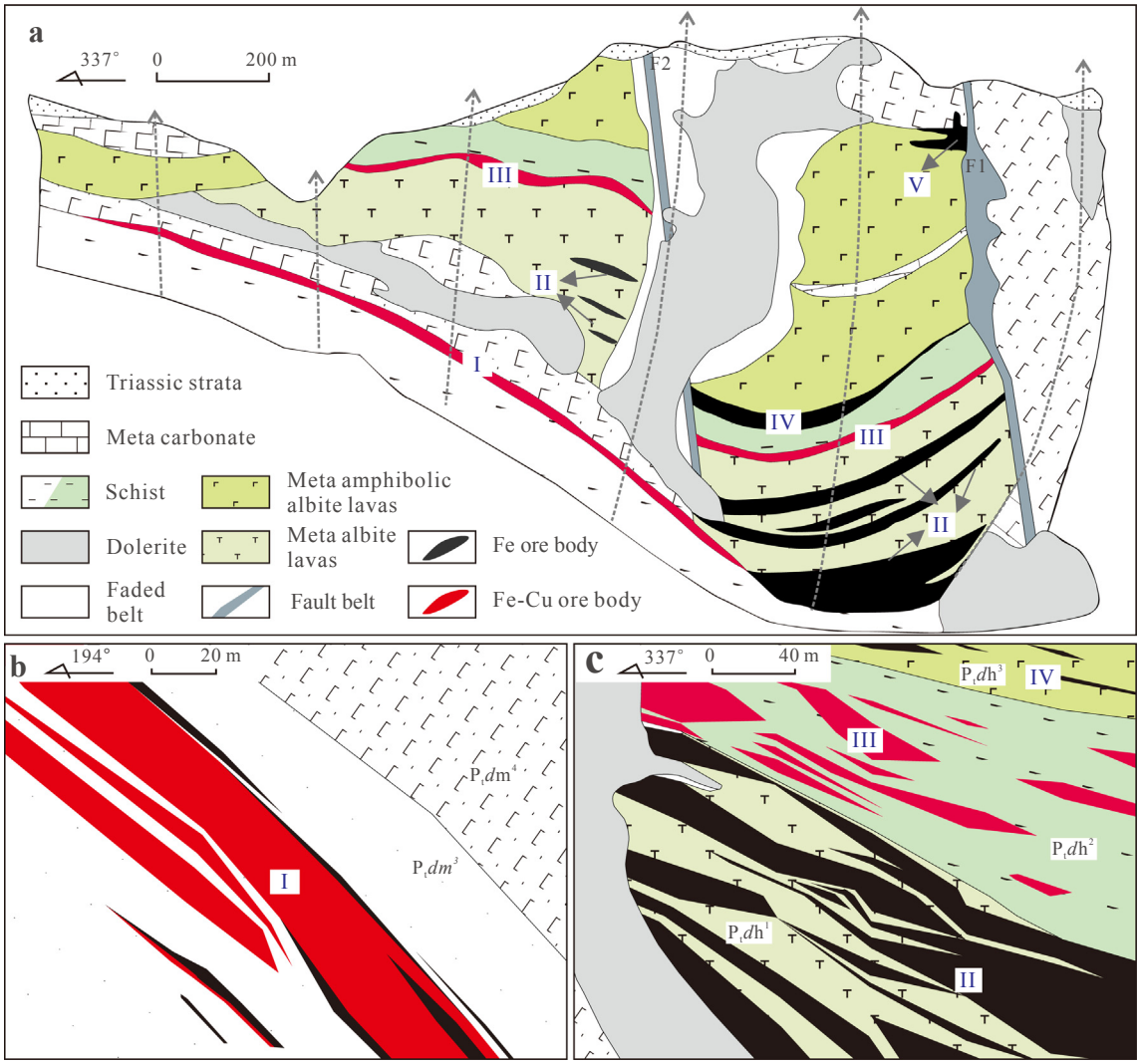

Fig. 2. (a) Geologic cross section of No.A32 exploration line of the Dahongshan district showing the distribution of Fe and Fe-Cu orebodies and the Dahongshan Group (modified from Qian and Shen, 1990); (b) Geologic cross section of No.CK52 exploration line showing the shape of Fe-Cu orebody No. I; (c) Geologic cross section of No. A34 exploration line showing the shape of orebodies No. II-IV and postdated mafic intrusions, which crosscut orebodies (modified from N9GBYBGMR, 1983). Dashed grey lines with arrow stand for drilling holes.

the ordinary and high-V ores was observed in terms of mineral assemblages and textures.

4. Sampling and analytical methods

Samples collected from important orebodies including No. I-IV as well as related volcanic rocks were prepared for trace element analyses on magnetite by LA-ICP-MS. In order to obtain reliable data for magnetite, carefully selected magnetite grains were mapped and quantitatively determined for composition using EPMA. Some ore samples have also been analyzed for bulk compositions.

Fourteen ore samples from both Fe and Fe-Cu orebodies were analyzed for major and trace elements. Major element compositions of representative ore samples were determined using X-ray fluorescence spectrometers (XRF) at ALS Chemex Co Ltd, Guangzhou. The analytical precision is better than 5%. Trace elements were obtained on a Perkin-Elmer Sciex ELAN DRC-e ICP-MS at the State Key Laboratory of Ore Deposit Geochemistry (SKLOG), Institute of Geochemistry of Chinese Academy of Sciences (IGCAS). Samples were processed according to procedures described by Qi and Grégoire (2000). Analytical precision is better than 10% for most elements.

Wavelength-dispersive X-ray (WDX) maps of sample DHS1531 were collected by an EPMA-1600 electron microprobe at SKLODG, IGCAS. BSE images were collected by a JSM-7800F field emission scanning electron microscope at SKLODG, IGCAS. Compositional analyses of representative magnetite to apply for LA-ICP-MS data reduction were conducted with a JOEL JXA 8230 wavelength dispersive electron microprobe at the School of Resources and Environmental Engineering, Hefei University of Technology, China.

Magnetite grains from different orebodies and the hosting mafic volcanic rocks were chosen for LA-ICP-MS trace element analyses. Measurements were performed using a Coherent GeoLasPro 193-nm Laser Ablation system coupled with an Agilent 7700x ICP-MS at the SKLODG, IGCAS. Detailed operating conditions for the same instrument and system have been presented in Gao et al. (2013). Helium was used as carrier gas and mixed with argon gas via a T-connector before measurement. A laser spot size of 44 μm and a repetition rate of 5 Hz were used for ablating both the unknowns and standards. Each analysis consists of 20 s on gas blank as the background, followed by 60 s analysis on sample. Standard materials including GSE-1G, BCR-2G, NIST 610, BC-28, and GOR-128 were applied in calibrating element contents with ^{57}Fe as the internal standard. GSE-1G with another standard was inserted in every eight unknown analyses to monitor time-dependent drift of sensitivity and mass discrimination. FeO values

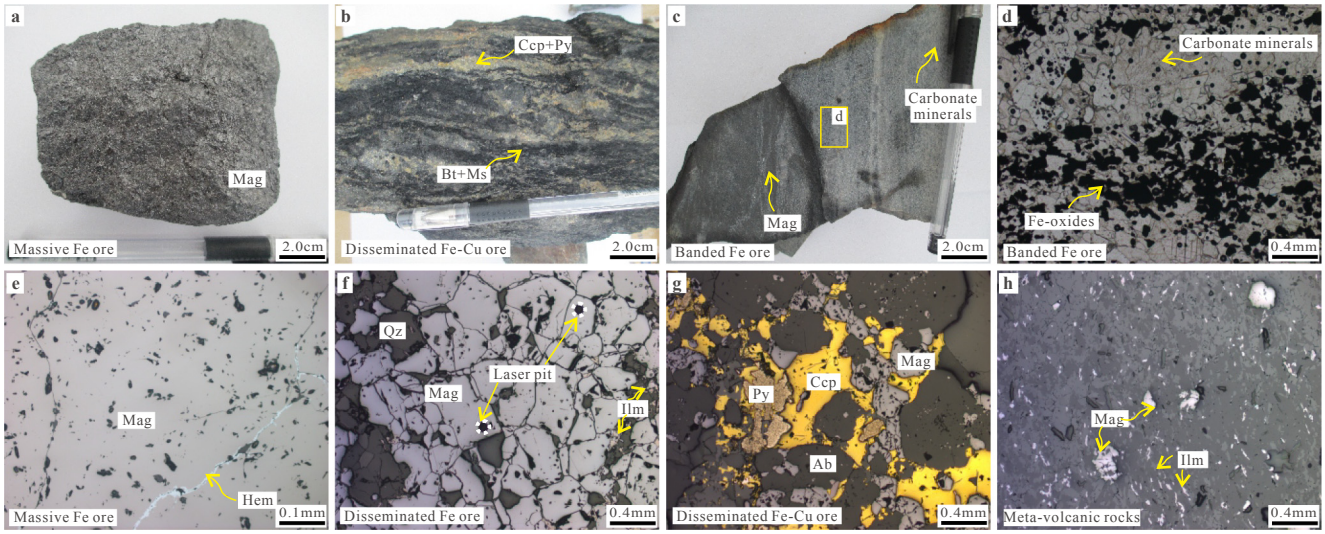

Fig. 3. Representative samples from the Dahongshan deposit. a) Massive magnetite from Fe orebody No. II; b) Disseminated sulfides from Fe-Cu orebody No. I; c) Banded magnetite from orebody No. III, which is in transition contact with carbonate (d). Photomicrographs of massive (e) and disseminated (f) magnetite ores, sulfides ores (g) and meta-volcanic rocks (h) from the Dahongshan deposit. Note that there is martitization along the fractures in massive magnetite. Abbreviations: *Ab* albite, *Ank* ankerite, *Bor* bornite, *Bt* biotite, *Ccp* chalcopyrite, *Mag* magnetite, *Ms* muscovite, *Py* Pyrite, *Qz* quartz.

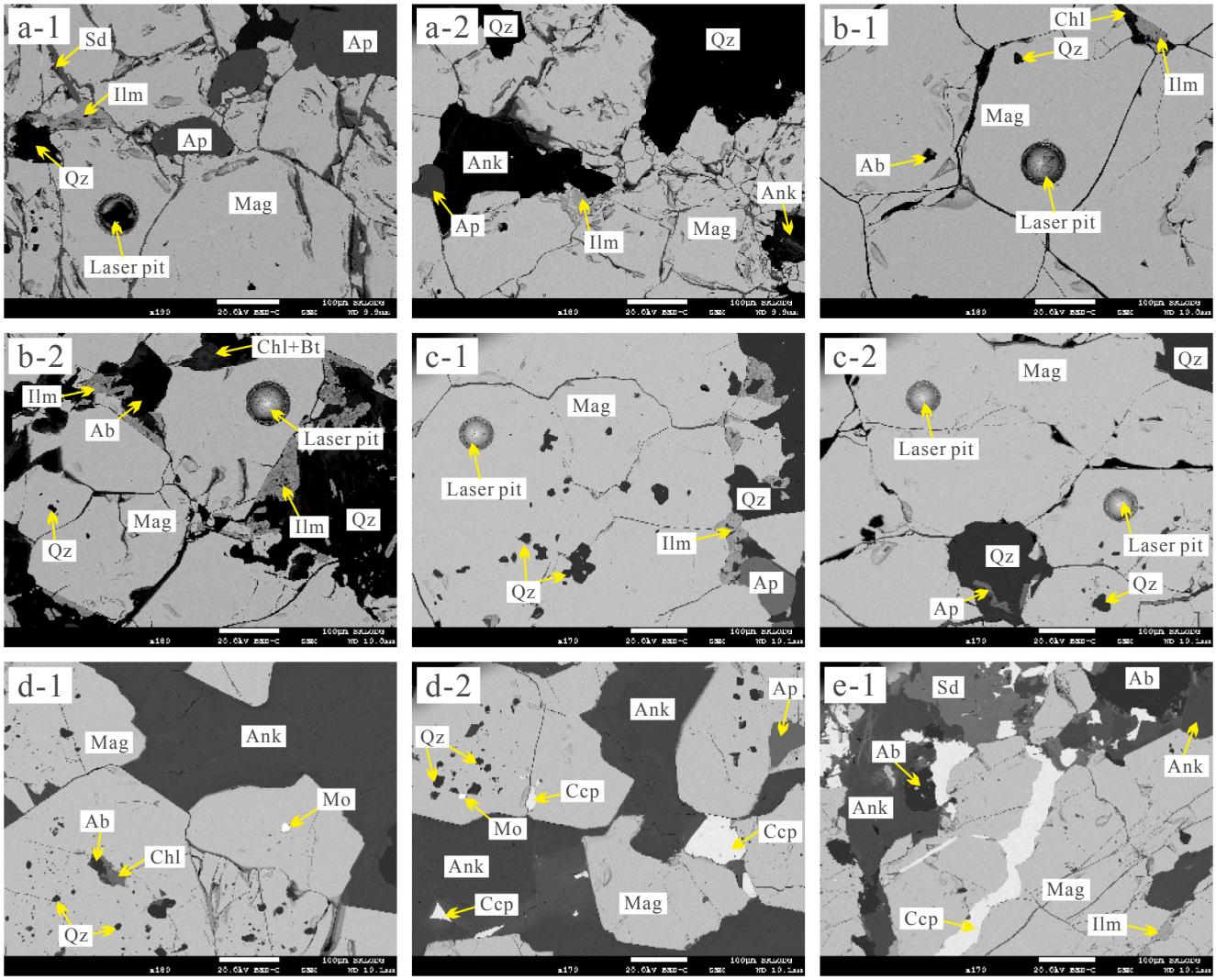

Fig. 4. Microscopic photos of representative ores from the Dahongshan deposit. Samples used for BSE study include DHS1518 (fig.a-1,a-2), DHS1611 (fig.b-1,b-2), DHS1612 (fig.c-1,c-2), DHS1605 (fig.d-1,d-2) and JKB52-1 (fig.e-1). Abbreviations: *Ab* albite, *Ank* ankerite, *Ap* apatite, *Bt* biotite, *Ccp* chalcopyrite, *Chl* chlorite, *Ilm* ilmenite, *Mag* magnetite, *Mnz* monazite, *Mo* molybdenite, *Py* Pyrite, *Qz* quartz, *Sd* siderite.

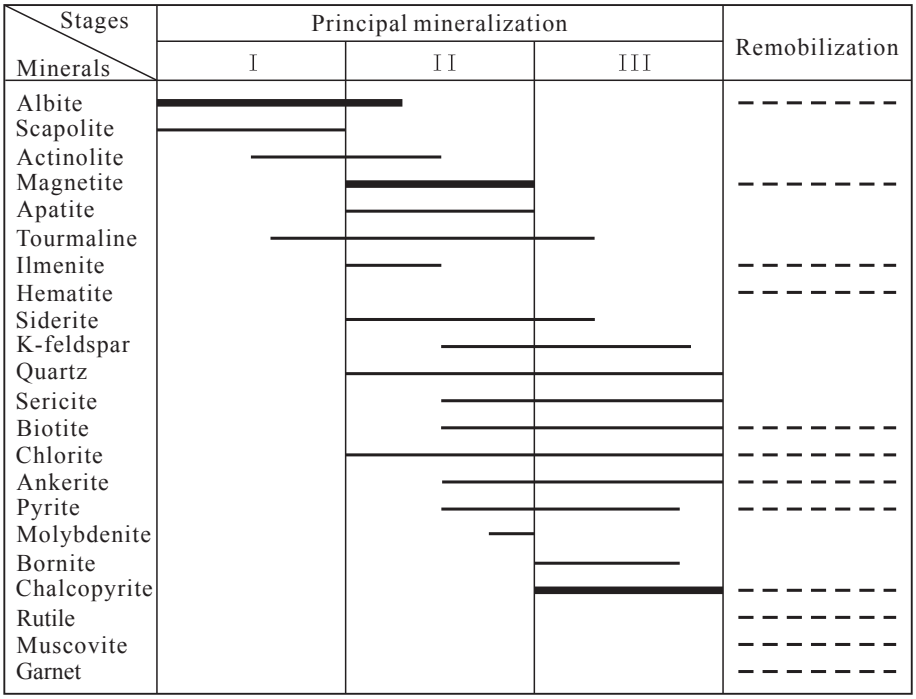

Fig. 5. Paragenetic sequence of ores in the Dahongshan deposit. Thick lines represent the most characteristic minerals in each stage.

determined by EPMA on representative magnetite were used for offline data reduction using ICPMSDataCal (Liu et al., 2008).

5. Analytical results

5.1. Bulk ore composition

Major and trace element compositions of ore samples are listed in Table 1. All of the analyzed ore samples show relatively high contents of $Fe_2O_3^T$ (55.7–99.5 wt%) and low contents of TiO_2 (< 1.03%). P_2O_5 contents of different orebodies range from 0.14 to 0.48 wt% (mostly at 0.4 wt%). Notably, three samples from orebody No. III have V contents (up to 3700–5320 ppm) an order higher than other samples (V = 62–270 ppm). Contents of other important metals (Co, Ni, Zn, and Mo) typically vary from several to tens of parts per million. For comparison purpose, rare earth element concentrations of ore samples without significant post-ore alterations are normalized against PAAS (Post-Archean Australian Shale) data. These ores samples (9 of 11 ordinary ores) show good linear relationships between major and trace elements with TiO_2, including the highly mobile elements like Na and Sr (not shown here), suggesting that their chemistry has not been insignificantly modified by post-ore hydrothermal overprinting events. These ores mainly show flat REE patterns (Pr/Yb_{SN}: 0.49–3.87, Avg. 1.29) with positive Eu anomalies (Eu^*_{SN}: 1.17–6.04, Avg. 3.49) but without significant Ce anomaly (Ce^*_{SN}: 0.92–1.03, Avg. 0.98) (Table 1, Fig. 6).

5.2. Mapping of ore samples

For the purpose of figuring out why V contents are extremely enriched in some ore samples, we mapped the distribution of primary elements using EMPA. Images in Fig. 7 show the distribution of Ti, V, Cr, Ni, and Si in magnetite. With abundant siderophile elements (Ti, V, and Ni) in magnetite and lithophile elements (Si) in silicates, it is clear that the enrichment in V and Cr of ore samples is caused by magnetite. Vanadium, Ni and Cr distributed homogeneously within magnetite grains. By contrast, Ti is slightly more enriched in main crystal plane (1 1 1) and fractures of magnetite.

5.3. Chemistry of magnetite

Data of magnetite analyzed by EMPA are presented in Table 2. All magnetite shows high FeO^T contents and overall low contents of TiO_2 and other elements. Trace element compositions of magnetite are supplied in Appendix I. Mineral inclusions may be responsible for enrichments of specific elements, for example, phosphates and sulfides contribute P, Ca, REE, S, and transition metals (Nadoll et al., 2014). These inclusions were carefully avoided in the offline data reduction. Magnetite from Fe and Fe-Cu orebodies has substantial Cr, Ni, V, Co, Ti, Zn, Ga, Mn, Mg, Al, Si, Sc and Sn, which are above detection limits and will be used for discussions below. Other elements such as Nb, Ta, Ge, Mo, Zr, Cu, Pb and W are close to or below limit of detection, so they will not be discussed further.

Magnetite grains from Fe and Fe-Cu orebodies hosted by both volcanic and sedimentary rocks have comparable ranges of Ga (~4–62 ppm), V (~56–11460 ppm), Cr (0–384 ppm), Al (~94–1126 ppm), Si (~189–3889 ppm), Mn (~8–261 ppm), Co (~3–125 ppm), Ni (~13–492 ppm), Mg (~4–282 ppm), and Sn (0–2.8 ppm)(Appendix I, Fig. 8).

Notice that V exhibits a range of ~56–1700 ppm for most magnetite grains and much higher ranges (~3365–5617 ppm, ~8237–11459 ppm) for some magnetite grains in orebodies. Except for the high-V samples, trace elements in magnetite of most ores show correlations with V contents. Specifically, Ni, Ga, Cr and Ti are positively and Mn, Sn Zn and Al are negatively related with V for magnetite of orebodies hosted in volcanic rocks. Ni, Ga, Cr and Zn are positively while Mn, Sn and Co are negatively related with V for magnetite of orebodies hosted in sedimentary rocks. Contents of Si remain unchanged with increasing V for all magnetite grains in orebodies (Fig. 8).

Magnetite from Fe and Fe-Cu orebodies are plotted in Ti + V vs. Al + Mn diagram (Dupuis and Beaudoin 2011; Nadoll et al., 2014). In Fig. 9a, most magnetite grains have low Al + Mn values and variable Ti + V values, and fall into the bottom of Kiruna, IOCG, BIF fields and areas below them. Several ore samples with extremely elevated V concentrations (~8237–11459 ppm, avg. 10203 ppm) plot within the Fe-Ti, V deposit field (Fig. 9a). All analyses share common feature of Ti and Ni/Cr values with magnetite from hydrothermal environment

Table 1
Major Element (in wt. %) and Trace Element (in ppm) compositions of ore samples from the Dahongshan deposit.

Sample no.	DHS1509	DHS1512	DHS1513	DHS1518	DHS1519	DHS1523	DHS1529	DHS1530	DHS1531	DHS1533	DHS1534	DHS1535	DHS1536	DHS1537
SiO_2	7.74	13.00	7.79	33.00	13.45	41.20	12.40	10.95	15.70	6.06	10.55	1.96	1.11	2.04
TiO_2	0.10	0.36	0.14	0.35	0.32	1.03	0.42	0.35	0.48	0.08	0.39	0.01	0.03	0.03
Al_2O_3	1.72	5.15	1.50	0.41	2.51	0.68	2.85	2.11	0.39	0.32	0.38	0.64	0.24	0.46
Fe_2O_3	89.6	76.7	90.6	57.0	79.1	55.7	76.7	80.8	81.0	93.7	88.9	96.8	99.5	97.2
MnO	0.04	0.07	0.02	0.06	0.15	0.02	0.28	0.29	0.03	0.02	0.01	0.01	0.03	0.01
MgO	0.49	0.70	0.53	1.32	1.74	0.31	1.21	0.81	0.46	0.25	0.07	0.25	0.20	0.12
CaO	0.76	1.66	0.66	3.37	1.78	0.75	2.86	2.63	1.40	0.58	0.30	0.75	0.84	0.37
Na_2O	0.26	0.33	0.48	0.01	0.61	0.20	1.47	0.95	0.06	0.03	0.12	0.18	0.02	0.16
K_2O	0.01	1.39	0.01	0.00	0.14	0.00	0.02	0.02	0.00	0.00	0.00	0.00	0.00	0.00
P_2O_5	0.14	0.20	0.36	0.45	0.22	0.36	0.23	0.21	0.42	0.16	0.19	0.48	0.42	0.24
Total	99.87	99.78	99.91	99.02	99.93	98.94	99.95	99.81	98.66	99.94	99.92	99.94	99.91	99.94
LOI.	−1.03	0.28	−2.17	3.05	−0.12	−1.28	1.51	0.74	−1.32	−1.28	−0.96	−1.17	−2.51	−0.7
Sc	3.09	5.93	4.02	8.07	6.78	8.05	5.07	3.59	7.74	2.88	2.95	1.68	5.61	2.88
V	242	235	270	3700	79	4130	78	62	5320	72	168	95	156	107
Cr	11.6	7.63	19.9	439	18.4	195	17.6	14.5	185	13.2	17.9	12.4	8.46	11.4
Co	83.3	35.9	52.3	42.5	97.3	41.7	68.7	65.0	63.1	46.8	20.7	38.4	62.6	21.3
Ni	86.9	56.8	68.5	63.9	27.2	73.4	18.7	18.3	97.0	62.2	84.5	53.9	133	30.6
Cu	56.9	152	13.3	29.6	3.84	13.0	6.31	326	4.30	3.70	4.23	0.74	1.01	2.26
Zn	23.9	9.42	16.2	17.7	29.5	26.3	15.1	17.4	17.1	22.1	28.4	11.6	8.96	4.68
Ga	11.9	14.0	24.5	31.5	6.37	30.2	4.92	5.37	45.4	7.25	8.21	6.95	18.5	4.86
Rb	0.52	38.60	0.26	0.22	7.18	0.25	0.47	0.66	0.05	0.13	0.12	0.21	0.07	0.04
Sr	6.92	14.4	5.12	18.2	11.4	7.41	9.25	14.2	7.59	2.88	2.37	3.57	5.48	2.38
Y	5.30	19.1	9.68	26.3	13.4	18.2	6.70	7.00	20.4	3.35	5.37	4.65	10.7	4.52
Zr	20.0	107	24.9	5.69	49.4	71.1	66.7	60.1	36.4	16.6	62.5	2.77	0.87	11.9
Nb	6.43	32.9	7.59	1.11	8.33	10.0	9.87	10.3	1.77	4.45	14.0	3.04	7.81	7.07
Mo	15.1	6.05	12.5	1.57	3.45	0.55	42.4	61.6	1.39	9.68	6.00	54.7	2.85	69.3
Sn	0.73	2.79	1.06	0.52	5.95	0.60	3.08	4.57	19.7	27.0	14.2	7.32	2.57	21.0
Cs	0.09	0.15	0.05	0.04	0.52	0.08	0.02	0.08	0.02	0.02	0.01	0.03	0.01	0.02
Ba	8.47	280	5.21	6.96	25.0	7.01	8.60	9.64	2.37	1.83	5.05	2.54	1.52	1.18
La	8.64	14.2	6.59	8.88	11.4	4.73	31.50	42.5	6.90	24.9	4.47	7.68	4.93	15.0
Ce	15.7	28.2	13.5	21.4	19.9	12.9	50.0	64.9	16.5	37.4	8.21	13.9	12.2	25.2
Pr	1.61	2.95	1.60	2.82	1.87	1.81	4.21	5.29	2.14	3.27	0.81	1.37	1.48	2.27
Nd	5.98	12.0	6.89	14.1	6.75	9.21	13.5	16.4	10.4	10.5	3.33	5.52	7.05	8.04
Sm	1.38	3.19	1.93	4.38	1.48	2.65	2.32	2.60	3.14	1.51	0.91	1.27	2.32	1.78
Eu	0.81	1.71	0.91	1.58	1.30	0.74	2.86	3.71	1.00	1.36	0.87	1.73	2.09	2.30
Gd	1.42	4.31	2.23	4.84	1.53	3.23	2.28	2.49	3.58	1.37	1.08	1.50	2.90	1.79
Tb	0.23	0.79	0.38	0.90	0.32	0.55	0.35	0.36	0.67	0.17	0.16	0.20	0.39	0.23
Dy	1.19	4.22	2.04	4.75	2.23	3.47	1.60	1.48	3.85	0.70	0.88	1.09	2.16	1.11
Ho	0.21	0.77	0.36	0.92	0.50	0.68	0.29	0.29	0.74	0.12	0.17	0.19	0.37	0.18
Er	0.63	2.09	0.97	2.58	1.57	1.75	0.86	0.92	1.90	0.36	0.49	0.50	0.99	0.50
Tm	0.08	0.34	0.13	0.29	0.24	0.23	0.11	0.13	0.25	0.05	0.06	0.07	0.11	0.05
Yb	0.53	2.23	0.66	1.70	1.48	1.19	0.81	0.85	1.24	0.27	0.37	0.31	0.62	0.39
Lu	0.07	0.31	0.09	0.24	0.21	0.16	0.12	0.13	0.15	0.04	0.05	0.04	0.06	0.04
Hf	0.46	2.47	0.61	0.20	1.14	1.91	1.63	1.45	0.77	0.30	1.30	0.10	0.05	0.33
Ta	0.21	1.60	0.30	0.06	0.31	0.58	0.47	0.51	0.11	0.14	0.39	0.04	0.28	0.13
Pb	2.68	1.02	0.22	1.94	5.18	1.72	4.38	3.76	0.73	1.28	1.47	1.17	0.39	1.01
Th	0.84	2.93	0.64	0.53	1.54	0.53	1.13	1.14	0.90	1.00	0.94	0.45	0.23	1.19
U	0.51	2.94	0.51	0.60	1.70	0.42	9.30	10.3	0.74	1.08	1.53	2.17	0.30	1.32
Ce^*_{SN}	0.97	1.00	0.96	0.98	0.97	0.95	0.92	0.99	0.98	1.03	0.97	0.97	0.99	0.98
Eu^*_{SN}	2.71	2.11	2.04	4.05	5.84	6.85	4.45	4.07	5.82	3.72	6.04	1.60	1.17	1.39
Pr/Yb_{SN}	0.97	0.42	0.77	0.40	1.66	1.99	3.87	0.70	1.41	0.76	1.86	0.53	0.49	0.55

SN = Post-Archean Australian Shale Normalized; $Ce^*_{SN} = 2*Ce_{SN}/(La_{SN} + Pr_{SN})$; $Eu^*_{SN} = 2*Eu_{SN}/(Sm_{SN} + Gd_{SN})$; $Pr/Yb_{SN} = Pr_{SN}/Yb_S$; LOI = Loss on Ignition.

(Fig. 9b; Dare et al., 2014).

Selected elements including Cr, Ni, V, Ti, Co, Ga, Mn, Sn, Zn, Sc, Al, Si, and Mg in magnetite from this study and references are normalized to bulk continental crust for comprehensive comparison (Fig. 10). Magnetite from orebodies shares comparable patterns in spider diagrams with spikes in Ga, Co and Ni, and valleys in Si and Mg, and variable Ti and V (Fig. 10a). Slight differences can also be observed. Variable concentrations of Ti are features of magnetite from the Fe orebodies (Fig. 10a). Magnetite from the Dahongshan deposit has patterns distinct from those of magmatic deposits, but similar to those of IOCG deposits in Australia (Fig. 11b and c).

6. Discussion

Hu et al. (2014, 2015) reported that equilibration processes would produce secondary magnetite with chemistry different from that of primary magnetite in skarn deposit. Because the Dahongshan deposit has suffered post-ore modification at 1.02 Ga and 0.83 Ga (Zhao et al., 2017), it is necessary to evaluate the potential effects of hydrothermal alteration on magnetite chemistry. As shown in Fig. 4, no texture of equilibration and replacement has been found in ore magnetite grains used for trace elements determination. Magnetite grains in Fig. 4b-1, b-2, c-1 have typical triple-junction texture, which is similar to that of primary magnetite from Forsyth deposit (Hu et al., 2015). Notice that magnetite in Fig. 5d-1, d-2 have some “core-rim” texture with abundant quartz and albite inclusions in the core. However, this distribution of inclusions contrasts with that of secondary magnetite caused by hydrothermal overprinting in Forsyth deposit (Hu et al., 2015) but coincides with that of primary magnetite from the Los Colorados iron deposit in Chile (Knipping et al., 2015a,b). Moreover, it has been suggested that V, Ga, Ni and Sn concentrations remain essentially unchanged during recrystallization and reequilibration processes (Hu et al., 2014, 2015). By contrast, elements such as Mn, Al, Si, Zn, Co and Ti behave as mobile elements during recrystallization and

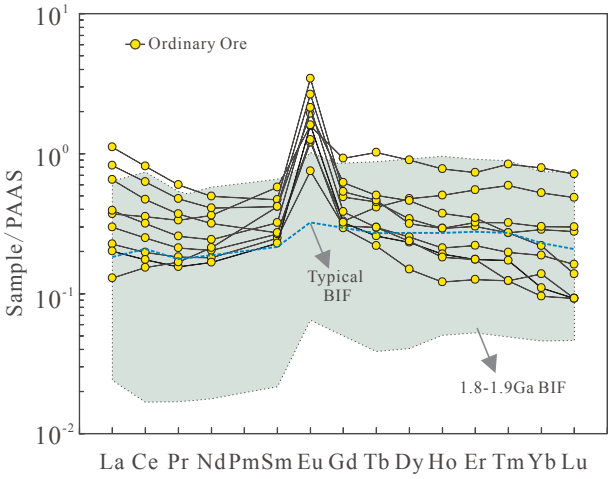

Fig. 6. Shale-normalized (PAAS) REE patterns for representative ore samples of the Dahongshan deposits. Ordinary ore samples come from orebodies No. II and III. Greenish area represents the 1.8–1.9 Ga BIF (Planavsky et al., 2010).

reequilibration processes and tend to decrease in concentrations within the secondary magnetite (Hu et al., 2014, 2015). However, linearly relationships between these elements with V contents argue against significant post-ore modification on magnetite compositions (e.g., magnetite in iron orebody hosted in carbonate; Fig. 8). Both microscopic and geochemical observations suggest that magnetite grains in this study have not been significantly changed by post-ore alterations.

6.1. Classification of magnetite

Elements such as Cr, Ti, Ni, and V have been used in various classification diagrams to distinguish between hydrothermal and magmatic magnetite (Dare et al., 2014; Knipping et al., 2015a; Nadoll et al., 2015). Contents of these elements are generally high in magmatic magnetite, but low in hydrothermal magnetite (Dare et al., 2014; Knipping et al., 2015a; Nadoll et al., 2015). Multi-element diagram normalized to bulk continental crust has been verified to work well in distinguishing trace element patterns among magmatic, high-T and low-T hydrothermal magnetite (Dare et al., 2014). Here we use multi-element diagrams, as well as empirical binary discrimination diagrams to provide integrated interpretation on magnetite in this study.

Magnetite from the Dahongshan deposit has low Ti + V contents and relative high Ni/Cr values (Fig. 9a, b), implying a hydrothermal origin. This is also evidenced by the multi-element diagrams (Fig. 10), in which the Dahongshan deposit has magnetite with trace elements contents overall much lower than those of the typical Bushveld and ELIP magmatic magnetite, especially in terms of Cr, Ti, Zn and Mn, but similar to those of hydrothermal magnetite grains from Ernest Henry and Lightening Creek deposits (IOCG) in Australia. Noteworthily, the presence of high-V magnetite from the Dahongshan deposit is very special as few cases have been reported on hydrothermal magnetite from economic deposits with such high level of V concentrations (~10000 ppm, comparable to those of magmatic magnetite). The contents of V in hydrothermal magnetite have a general range of ~10–4000 ppm (Nadoll et al., 2015), and the high-V magnetite in the Dahongshan deposit is far beyond the general range of V in hydrothermal magnetite (~10–4000 ppm; Nadoll et al., 2015). Interestingly, the high-V magnetite grains have identical Ni/Cr ratios and Ti values to the hydrothermal magnetite and are different from those of magmatic

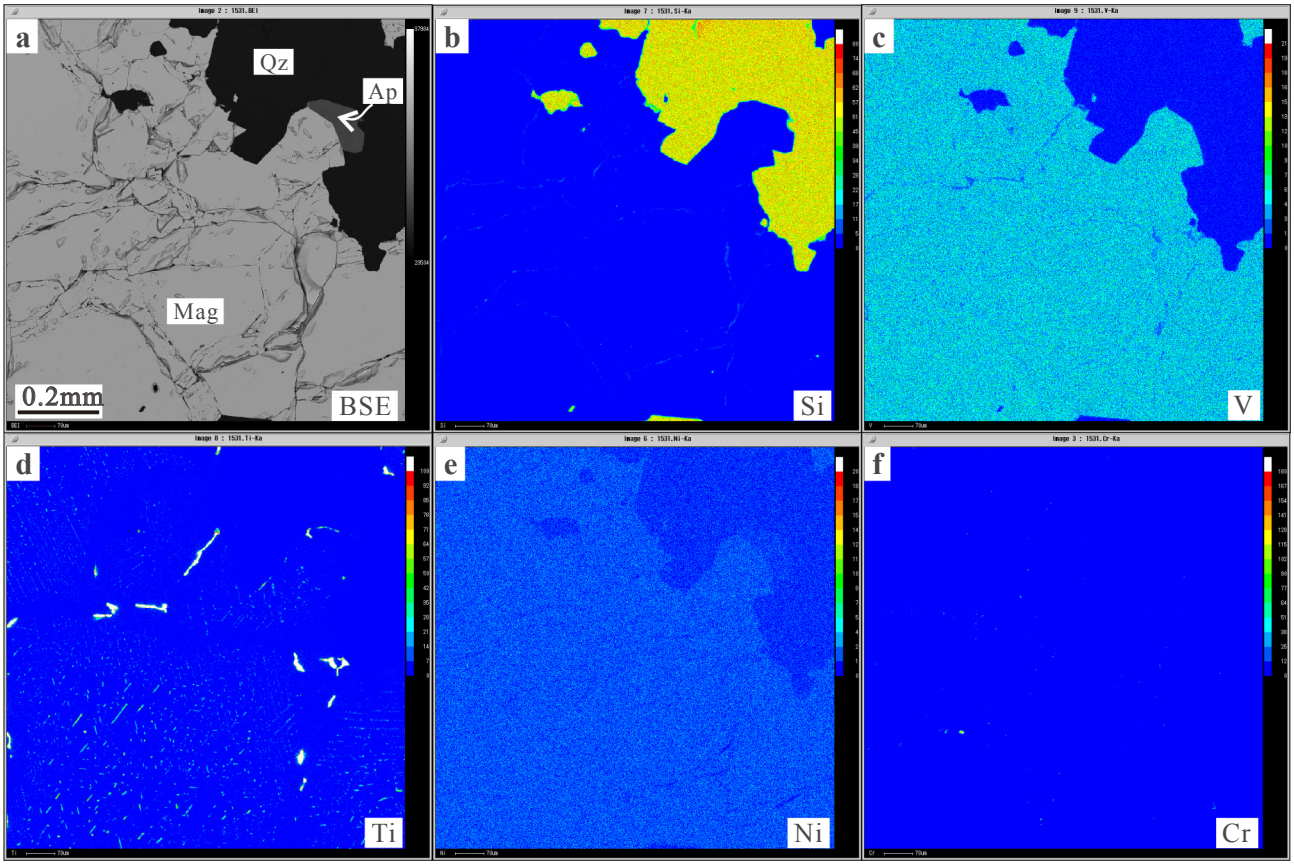

Fig. 7. BSE (a) and WDS elemental maps of selected elements (b-f: Si, V, Ti, Ni and Cr) in the high-V magnetite grains. Notice that V shows homogenously high contents in magnetite, whereas other elements (Si, Ti, Ni and Cr) have relatively low abundances in magnetite grains.

Table 2
Chemical compositions (wt. %) of the representative magnetite grains from ore samples andaltered volcanic rocksof the Dahongshan deposit.

Sample	JKB52-7	JKB52-1	CK34-15	DHS1535	DHS1633	CKN5-26	CKN5-12	DHS1513	DHS1523	DHS1531
Ore body No.	I	I	II-1	II-2	II-5	III-1	IV	III-2	III-2	III-2
Wall Rock	Schist	Schist	Volcanic rocks	Volcanic rocks	Volcanic rocks	Schist	Volcanic rocks	Carbonate	Carbonate	Carbonate
n	8	8	8	5	8	8	8	12	8	8
MgO	0.01	0.00	0.00	0.02	0.01	0.01	0.02	0.01	0.00	0.00
Al_2O_3	0.16	0.11	0.06	0.13	0.05	0.12	0.10	0.09	0.08	0.13
TiO_2	0.05	0.05	0.00	0.00	0.00	0.00	0.00	0.13	0.03	0.02
CaO	0.00	0.00	0.00	0.00	0.00	0.00	0.00	0.00	0.00	0.00
K_2O	0.00	0.00	0.00	0.00	0.00	0.00	0.00	0.01	0.00	0.00
Cr_2O_3	0.02	0.02	0.01	0.01	0.03	0.03	0.02	0.02	0.07	0.10
Ga_2O_3	0.02	0.03	0.02	0.05	0.04	0.01	0.02	0.07	0.02	0.05
P_2O_5	0.02	0.01	0.01	0.01	0.01	0.01	0.00	0.01	0.01	0.00
Na_2O	0.01	0.01	0.00	0.01	0.00	0.01	0.01	0.01	0.01	0.01
SiO_2	0.03	0.02	0.01	0.05	0.01	0.08	0.05	0.03	0.05	0.02
V_2O_3	0.06	0.66	0.05	0.02	0.04	0.11	0.21	0.01	1.45	1.22
MnO	0.01	0.01	0.00	0.00	0.01	0.01	0.00	0.00	0.00	0.03
FeO	31.13	31.06	31.06	31.32	30.97	31.08	30.94	31.30	31.15	31.07
Fe_2O_3	68.72	68.21	69.08	69.43	68.90	68.67	68.67	68.87	67.39	67.61
CoO	0.11	0.11	0.12	0.04	0.11	0.10	0.14	0.04	0.12	0.10
NiO	0.01	0.03	0.01	0.01	0.00	0.01	0.05	0.01	0.02	0.00
CuO	0.00	0.00	0.00	0.02	0.00	0.00	0.00	0.01	0.00	0.00
Total	100.36	100.31	100.46	101.12	100.19	100.25	100.23	100.61	100.41	100.37
Fe^{2+}/Fe^*	0.33	0.34	0.33	0.33	0.33	0.33	0.33	0.34	0.34	0.34

Note: Fe_2O_3 calculated on the basis of stoichiometry.

magnetite (Fig. 9b). In the multi-element diagrams of magnetite (Fig. 10), trace elements of the Dahongshan deposit overall show much lower contents than those of typical magmatic ores, especially in terms of Cr, Ti, Zn and Mn. Notice that the high-V magnetite grains overlap with magmatic magnetite in V and Ga, but show much more features different from them.

In summary, the spider diagrams support a hydrothermal origin for magnetite in the Dahongshan deposit, including the unique high-V magnetite.

6.2. Factors influencing geochemistry of hydrothermal magnetite from ordinary ores

The most important factors governing trace element compositions in hydrothermal magnetite include (1) nature of fluids, e.g., fluids chemistry, and physiochemical conditions (such as T and fO_2), (2) wall rock buffering, and (3) coprecipitating minerals and so on (Carew, 2004; Dupuis and Beaudoin, 2011; Dare et al., 2014; Nadoll et al., 2014). It is essential to discuss the potential effects of each factor to reach an integrated understanding on the formation of magnetite and orebodies.

6.2.1. Wall rock buffering

Wall rock buffering is an important control to change the geochemical composition of precipitated hydrothermal magnetite (Nadoll et al., 2014). Different wall rock might result in fluids enriched in special elements. Fluids experienced extensive fluid-rock interactions in skarn deposit show high contents of Mg and Mn and form hydrothermal magnetite inheriting the enrichment of both Mg and Mn (Nadoll et al., 2014 and references therein). Rusk et al. (2010) attributed the different concentrations of V and Mn in magnetite from Ernest Henry to the mineral-fluid equilibrium when magnetite was deposited (Rusk et al., 2010). Mafic-ultramafic rocks were introduced to explain the high Ni contents of magnetite from some BIF deposits (Angerer et al., 2012). Different wall rocks will be discussed below to evaluate their effect on magnetite chemistry.

Magnetite hosted in meta-volcanic rocks has slightly higher contents of Ni than that in meta-sedimentary rocks at certain vanadium concentrations (Fig. 8a). This could be caused by the contribution of mafic minerals of meta-volcanic rocks. However, other elements like Cr and Ti argue against significant fluid-rock interaction, because (1) Cr shows comparable variations in magnetite from meta-volcanic rocks and meta-sedimentary, and (2) Ti is relatively enriched in magnetite grains hosted in meta-sedimentary rocks rather than meta-volcanic rocks. Moreover, Mg and Mn in magnetite grains hosted in carbonate overlap with those magnetite grains hosted in schist and meta-volcanic rocks (Fig. 11), which implies the fluid-rock interaction between ore-forming fluids and carbonate contribute little to the compositional variation of magnetite. Most elements in magnetite are not correlated with wall rock compositions. Therefore, magnetite chemistry is not mainly controlled by fluid-rock interaction.

6.2.2. Coprecipitating minerals

Minerals co-precipitating with magnetite may have considerably higher partition coefficients for some elements than magnetite, thus leading to lower contents of those elements in magnetite (Dare et al., 2014; Nadoll et al., 2014; Chen et al., 2015). The Fe-oxide stage in the Dahongshan deposit has a simple mineral assemblage of magnetite, ilmenite, albite, quartz, apatite and some siderite and ankerite, with minor hematite. The Cu-sulfide stage displays mineral assemblage of magnetite, chalcopyrite, with or without pyrite, albite and carbonate. Locally, minor molybdenite precipitated with magnetite. Gangue minerals, such as albite, apatite and quartz, generally show much lower contents of Ti, Cr, V, Ni, Co, Cu, Mo, Mn, Mg and Zn than that in magnetite (Neilson, 2003), indicating that composition of magnetite may not be notably affected by the gangue minerals. Both carbonate minerals and magnetite can incorporate Mn and Mg. However, whether siderite and ankerite arise seems to have limited correlations with the Mn and Mg variations in magnetite hosted by carbonate rocks (Figs. 4a–e, 8e). Hematite grains formed by martitization would not change the composition of magnetite. Dare et al. (2014) reported that the chalcophile elements are depleted in magnetite grains which are co-precipitated with sulfides. Minor sulfides co-precipitated with magnetite in the Dahongshan deposit. This may provide explanation for the depletion trend of Zn in magnetite hosted by carbonate (Fig. 9h). However, several lines of evidence argue against such interpretation. Sulfides coexisting with magnetite are (1) primarily molybdenite, which is generally not enriched in Zn, and (2) limited in amount. Moreover, other chalcophile elements (e.g., Co, and Sn) are enriched in magnetite bearing molybdenite. It is less likely that these minor sulfides could have significant effects on magnetite chemistry. Reasons for the depletion trend of Zn in magnetite hosted by carbonate are unclear.

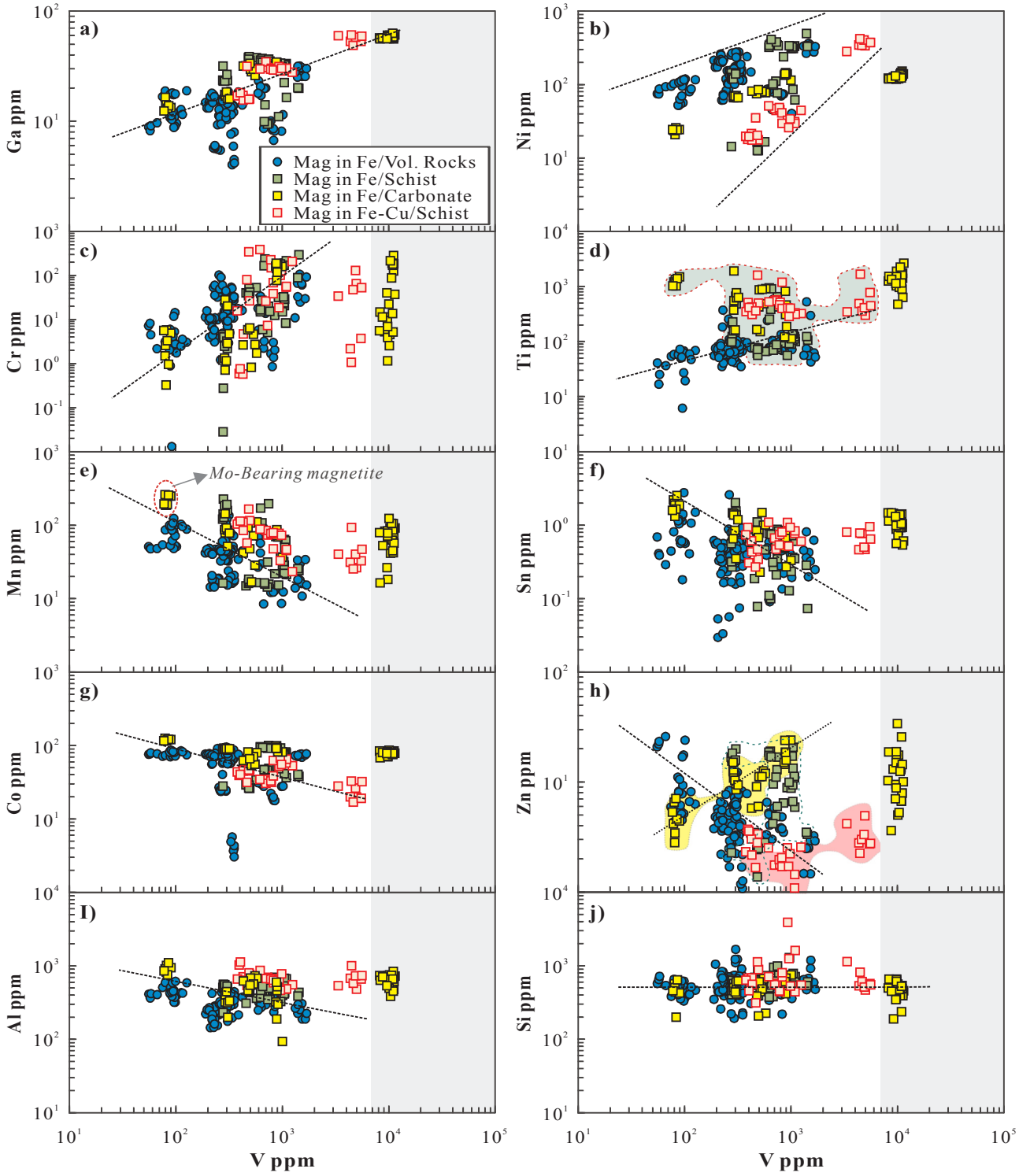

Fig. 8. Covariation of Ga, Ni, Cr, Ti, Mn, Sn, Co, Zn, Al and Si with V in magnetite grains from different orebodies. Blue circles represent magnetite from Fe orebodies (II, IV) in volcanic rocks. Yellow, green and red squares stand for magnetite from orebodies No. III-2, III-1 and I, respectively, all of which are hosted in sedimentary rocks. Greenish area in d is plots from orebodies hosted by meta-sedimentary rocks. The greyish areas aim to show the high-V magnetite is different from that in the ordinary ores. Dark dashed lines show general relationships between V and other elements. *Mo* is representative of molybdenite. (For interpretation of the references to colour in this figure legend, the reader is referred to the web version of this article.)

In summary, both wall rock buffering and coprecipitating minerals have negligible effects on chemical variations of magnetite in the Dahongshan deposit. In other words, chemistry of magnetite is primarily controlled by the chemistry and physiochemical conditions of fluids and in turn could provide constraints on nature of iron mineralizing fluids.

6.3. Implications for the nature of ore-forming fluids

To first order, magnetite should reflect the chemistry of ore-forming fluids. Magnetite grains from different iron (Fe) orebodies share both similar normalized trace element patterns and intimate trends of concentration of most trace elements with those of Fe-Cu orebodies,

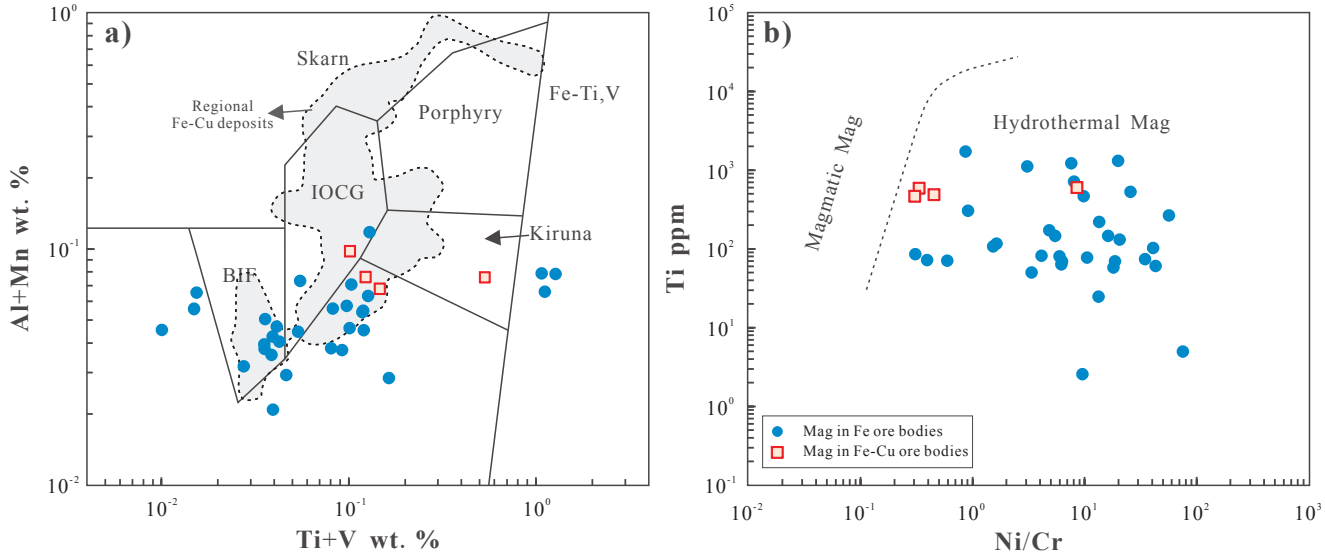

Fig. 9. (a) Chemical discrimination diagram for magnetite from different type deposits after Dupuis and Beaudoin (2011) modified by Nadoll et al. (2014). (b) Chemical discrimination diagram for magnetite from magmatic and hydrothermal environments after Dare et al. (2014). Every plotted point represents the average composition of about eight analyses from same thin slice. Regional Fe-Cu deposits data are from Chen et al. (2015).

particularly in terms of V, Cr, Ni, Co, Mg, Mn, Ga, Sn, Sc, Al and Si. These observations suggest that the fluids responsible for iron-related mineralization in Fe and Fe-Cu orebodies are chemically similar and may be cogenetic. However, magnetite from orebodies hosted in carbonate and schist is relatively enriched in Ti. Ilmenite grains also occur along with magnetite. For this reason, it is believed that iron-related mineralizing fluids for orebodies in meta-sedimentary rocks are relatively Ti-rich. Reason for this distinction is still unclear.

Similar to magmatic systems, intensive parameters, such as T and fO_2, may contribute to compositional variation of hydrothermal magnetite, but the process remains poorly understood (e.g., Ilton and Eugster, 1989; Toplis and Corgne, 2002; Nadoll et al., 2014). As shown in microscopic observation, minor molybdenite occur at the end of iron mineralization stage. This is indicative of a gradual reduced-towards transition in the mineralizing fluids with precipitation of magnetite. This is expected because (1) Fe is the major valence-variable element in such fluids and (2) magnetite preferentially incorporates Fe^{3+} over Fe^{2+} into its structure (e.g., Liang et al., 2009). Although fO_2 decreases with evolution, it seems to have negligible effects on compositions of magnetite for the ordinary ores. Vanadium (V) substitutes Fe^{3+} with +3, +4 and +5 valence states in magnetite and preferentially with the trivalent state (Toplis and Corgne, 2002), so the decreasing fO_2 increase compatibility of V with magnetite. Whereas tin (Sn) exhibits opposite behavior with V. However, magnetite coexisting with molybdenite are featured with lower V but higher Sn contents than that without molybdenite grains (Fig. 8f), inconsistent with significant influence of fO_2 on chemistry of magnetite from the ordinary ores. Similar conclusion was also reached in the study of magnetite from the Lala deposit (Chen et al., 2015). Moreover, the positive correlation of V and Ni, which is a homovalent cation, in each orebody might reflect that other factors rather than fO_2 control concentration of the valence-variable elements in magnetite.

It has been reported that Cu, Cd, Zn and Mn are preferentially concentrated into the evolved, lower temperature fluids in an experimental system composed of magnetite and supercritical chloride-rich fluids, and conducted at 600–800 °C at 2 kb (Ilton and Eugster, 1989). There are also observations on significant decrease in Ni, V, Ga and Ti from high-T to low-T hydrothermal magnetite (Nadoll et al., 2014; Knipping et al., 2015b). Our analyses on magnetite have two features: (1) a clustered range of V for each ore sample and (2) generally trends between V and other elements for ores from the same orebody (e.g., magnetite in iron orebody hosted in carbonate; Fig. 8). To be specific, Ni, Ga and Cr show broadly or strictly positive relations with V in all magnetite, while Mn, Sn and Co contents are negatively correlated with V contents in magnetite grains. For orebody hosted in carbonate, later magnetite grains (molybdenite-bearing) are enriched in Mn and depleted in Ga, Cr and Ni relative to earlier magnetite (Fig. 8). This likely reflects that temperature has inserted great effects on magnetite compositional differentiation via changing partition coefficients of elements into magnetite.

In summary, ore-forming fluids for iron-mineralization of Fe and Fe-Cu orebodies are chemically similar, even though orebodies in meta-sedimentary rocks were formed by relatively Ti-rich fluids. The evolved fluids are featured by lower fO_2 and T, and chemistry of magnetite recorded great influence from temperature.

6.4. Origin of high V magnetite

High-V magnetite bearing ores were collected from the Fe (-Cu) orebody hosted in carbonate rocks and are banded in shape. They are not in veins and are undistinguishable from ordinary ores of the same orebody in the field. We would like to emphasize that the high-V magnetite formed high-V ores at least in hand specimen scale based on homogenous elemental maps and magnetite chemistry. No high-V magnetite has been found in ordinary ores from the same orebody, and in return no ordinary magnetite occurs in the high-V ores. It is likely the high-V ores distributed within ordinary ores as concentrated zones.

If high-V magnetite bearing and ordinary ores were formed by different mineralization events, they would be expected to have distinct chemistry, textures and mineral association. However, no essential difference between the high-V magnetite bearing ores and ordinary ores has been observed concerning about the mineral association and microscopic textures (Fig. 4). Apart from higher V contents, the high-V magnetite has chemistry comparable with the that of magnetite in ordinary ores. This most likely reflects that they precipitated from similar fluids. The extremely high V in some magnetite grains could be readily attributed to locally extremely low fO_2, which would greatly increase compatibility of V into magnetite structure (Jedwab et al., 1989; Toplis and Corgne, 2002; Bordage et al., 2011).

Notice that not many cases have been reported on such high level of V in hydrothermal magnetite (up to 10000 ppm), which indicates that such extremely oxygen fugacity conditions should be scarce. As far as

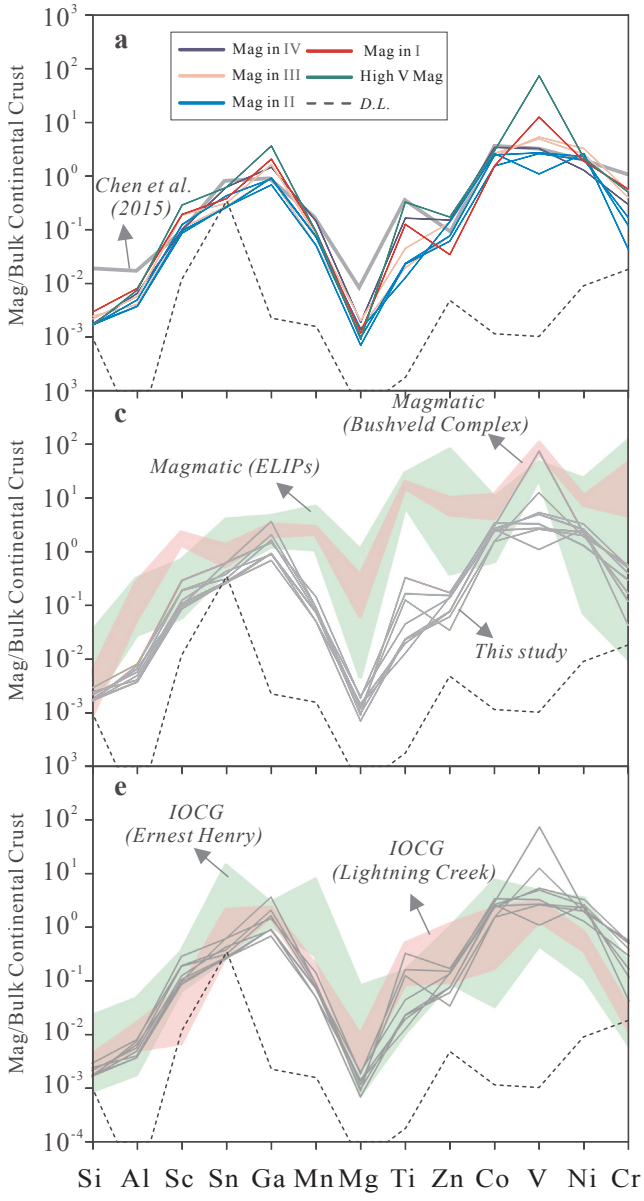

Fig. 10. (a) Multi-element variation diagrams for magnetite from Fe orebodies (II, III, IV, High-V magnetite), Fe-Cu orebodies (I) and meta-volcanic rocks in the Dahongshan deposit; (b-f) Comparisons of magnetite from the Dahongshan deposit with those of magmatic and IOCG deposits. Selected elements above detection limits are in order of increasing compatibility into magnetite from left to right according to Dare et al. (2014, 2015). Normalizing values are bulk continental crust from Rudnick and Gao (2003). Every line represents the average composition of analyzed orebody. Literature data are cited from Dare et al. (2014) and references therein for magmatic (Bushveld Complex), Carew (2004) for IOCG deposits, and Liu et al. (2015) for magmatic deposit (ELIPs).

we know, a study about the Red Sea has documented similar high-V magnetite (V = 9860 ppm) within carbonate sequences (Jedwab et al., 1989). Another case study on hydrothermal magnetite with high contents of V (~8500 ppm) comes from some iron ore deposits in northwestern China, in which seafloor conditions are the major ore-forming environment (Zhou et al., 2017). This scenario allows us to interpret that highly reduced marine environment is crucial for the generation of high-V magnetite. The absence of high-V magnetite in orebodies hosted by rocks other than carbonates actually provides insights into the significance of carbonate. A likely explanation is that massive input of terrigenous sediment and volcanic rocks would interrupt such highly reduced conditions favoring the generation of high-V magnetite. In

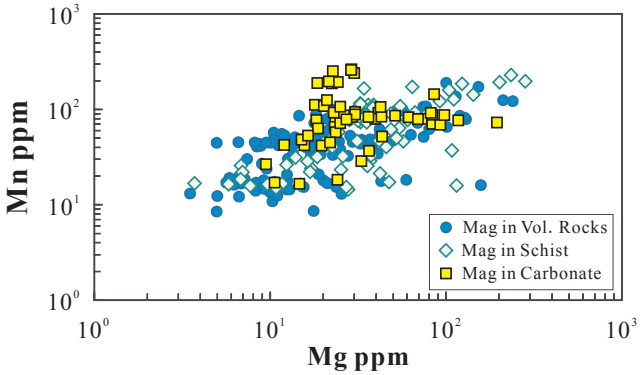

Fig. 11. Bimodal plots of Mn vs. Mg in magnetite grains from different country rocks including volcanic, schist and carbonate rocks.

summary, the high-V magnetite was generated in specially reduced, submarine environments like the Red Sea.

6.5. Models for the Dahongshan deposit

Zhao et al. (2017) suggested that the Dahongshan deposit is one of typical IOCG deposits in SW China. However, Kou et al. (2017) noticed that the deposit failed to meet the criteria for determination of the IOCG (Hitzman et al., 1992; Williams et al., 2005) in terms of lacking of significant Cu mineralization within Fe ore belts. Although magnetite from the Dahongshan deposit has geochemistry similar to that of IOCG deposits in Australia (this study), geological observations do not provide evidence for the IOCG model proposed by Zhao et al. (2017). Firstly, massive orebodies (at least iron orebodies) were crosscut by mafic intrusions (Qian and Shen, 1990; Kou et al., 2017; Zhao et al., 2017), precluding genetic relationship between them. Only small orebodies like orebody V, which is in irregular shapes, show temporally and spatially affinities with mafic intrusions (Qian and Shen, 1990; Zhao et al., 2017). Moreover, both the Fe and Fe-Cu orebodies are stratiform or stratiform-like in shape (Qian and Shen, 1990), which are typical feature of syn-sedimentary mineralization (Kou et al., 2017). Furthermore, this study also suggests submarine environments supporting the volcanic-hosted model for the deposit based on several lines of evidence below. (1) Whole rock REE patterns of ores in the Dahongshan deposit display large positive Eu anomaly without significant Ce anomaly, which are comparable to those of BIF deposit. Their large Eu enrichments are common feature of in the Proterozoic marine sedimentary rocks (Bekker et al., 2010). The deficiency of Ce anomaly and LREE/HREE ratio close to the shale composite value suggest low fO_2 in the site of ore deposition (Bekker et al., 2010). (2) The unique occurrence of high-V magnetite with carbonated layers indicates that the Dahongshan deposit was formed in environments like the Red Sea. Therefore, this study tends to support the volcanic-hosted model for the generation of the Dahongshan deposit (e.g., Qian and Shen, 1990; Kou et al., 2017).

7. Concluding remarks

Fluids formed the magnetite grains both in Fe and Fe-Cu orebodies of the Dahongshan deposit in SW China are likely chemically similar and cogenetic, although minor distinction might exist. Generally, the ore-forming fluids show reduced and low-temperature towards evolution, precipitating magnetite with gradual lower Cr, Ni, V, Ga contents but higher Mn, Sn, Co concentrations. The unique occurrence of Rea Sea-like high-V magnetite indicates locally highly-reduced marine environments for the deposit.

Declaration of Competing Interest

The authors declare that there are no competing financial interests or personal relationships that may have potential influence on the work reported in this paper.

Acknowledgments

This study was financially supported by the National Natural Science Foundation of China (Grants Nos. 41572074 and 41273049) and the Strategic Priority Research Program of the Chinese Academy of Sciences (Grant No. XDB18030204). We thank Zhihui Dai for her assistance on magnetite analyses using LA-ICP-MS. Much appreciation is also given to Jing Hu, Guangping Bao, and Yan Huang for their guidance in whole-rock chemical analysis. Juan Wang is specially acknowledged for her timely EMPA laboratory support.

Appendix A. Supplementary data

Supplementary data to this article can be found online at https://doi.org/10.1016/j.oregeorev.2020.103361.

References

Angerer, T., Hagemann, S.G., Danyushevsky, L.V., 2012. Geochemical evolution of the banded iron formation-hosted high-grade iron ore system in the Koolyanobbing greenstone belt, Western Australia. Econ. Geol. 107, 599–644.

Bekker, A., Slack, J.F., Planavsky, N., Krapez, B., Hofmann, A., Konhauser, K.O., Rouxel, O., 2010. Iron formation: the sedimentary product of a complex interplay among mantle, tectonic, oceanic, and biospheric processes. Econ. Geol. 105, 467–508.

Bordage, A., Balan, E., Villiers, J.R., Cromarty, R., Juhin, A., Carvallo, C., 2011. V oxidation state in Fe-Ti oxides by high-energy resolution fluorescence-detected X-ray absorption spectroscopy. Phys. Chem. Miner. 38, 449–458.

Carew, M.J., 2004. Controls on Cu-Au mineralization and Fe oxide metasomatism in the Eastern Fold Belt, N.W. Queensland, Australia. Ph.D thesis, James Cook University, Queensland.

Chen, W.T., Zhou, M.F., 2012. Paragenesis, stable isotopes, and molybdenite Re-Os isotope age of the Lala iron-copper deposit, Southwest China. Econ. Geol. 107, 459–480.

Chen, W.T., Zhou, M.F., Gao, J.F., Hu, R.Z., 2015. Geochemistry of magnetite from Proterozoic Fe-Cu deposits in the Kangdian metallogenic province, SW China. Miner. Deposita DOI: 10.1007/s00126-014-0575-7.

Chen, W.T., Zhou, M.F., Zhao, X.F., 2013. Late Paleoproterozoic sedimentary and mafic rocks in the Hekou area, SW China: implication for the reconstruction of the Yangtze Block in Columbia. Precambr. Res. 231, 61–77.

Dare, S.A.S., Barnes, S.J., Beaudoin, G., 2012. Variation in trace element content of magnetite crystallized from a fractionating sulfide liquid, Sudbury, Canada: implications for provenance discrimination. Geochim. Cosmochim. Acta 88, 27–50.

Dare, S.A.S., Barnes, S.J., Beaudoin, G., 2015. Did the massive magnetite “lava flows” of El Laco (Chile) form by magmatic or hydrothermal processes? New constraints from magnetite composition by LAICP-MS. Miner. Deposita 50, 607–617.

Dare, S.A.S., Barnes, S.J., Beaudoin, G., Meric, J., Boutroy, E., Potvin-Doucet, C., 2014. Trace elements in magnetite as petrogenetic indicators. Miner. Deposita DOi: 10.1007/s00126-014-0529-0.

Dupuis, C., Beaudoin, G., 2011. Discriminant diagrams for iron oxide trace element fingerprinting of mineral deposit types. Miner. Deposita 46, 319–335.

Fan, H.P., Zhu, W.G., Li, Z.X., Zhong, H., Bai, Z.J., He, D.F., Chen, C.J., Cao, C.Y., 2013. Ca. 1.5 Ga mafic magmatism in South China during the break-up of the supercontinent Nuna/Columbia: the Zhuqing Fe-Ti-V oxide ore-bearing mafic intrusions in western Yangtze Block. Lithos 168–169, 85–98.

Gao, J.F., Zhou, M.F., Lightfoot, P.C., Wang, C.Y., Qi, L., Sun, M., 2013. Sulfide saturation and magma emplacement in the formation of the Permian Huangshandong Ni-Cu sulfide deposit, Xinjiang, northwestern China. Econ. Geol. 108, 1833–1848.

Geng, Y.S., Kuang, H.W., Liu, Y.Q., Du, L.L., 2017. Subdivision and correlation of the Mesoproterozoic stratigraphy in the western and northern margins of Yangtze Block. Acta. Geol. Sin. 10 (91), 2151–2174 (in Chinese with English abstract).

Greentree, M.R., Li, Z.X., 2008. The oldest known rocks in south-western China: SHRIMP U-Pb magmatic crystallization age and detrital provenance analysis of the Paleoproterozoic Dahongshan Group. J. Asian Earth Sci. 33, 289–302.

Greentree, M.R., Li, Z.X., Li, X.H., Wu, H.C., 2006. Late Mesoproterozoic to earliest Neoproterozoic basin record of the Sibao orogenesis in western South China and relationship to the assembly of Rodinia. Precambr. Res. 151, 79–100.

Hitzman, M.W., Oreskes, N., Einaudi, M.T., 1992. Geological characteristics and tectonic setting of Proterozoic iron oxide (Cu-U-Au-REE) deposits. Precambr. Res. 58, 241–287.

Hou, L., Ding, J., Deng, J., Peng, H.J., 2015a. Geology, geochronology, and geochemistry of the Yinachang Fe-Cu-Au-REE deposit of the Kangdian region of SW China: evidence for a Paleo-Mesoproterozoic tectono-magmatic event and associated IOCG systems in the western Yangtze Block. J. Asian Earth Sci. 103, 129–149.

Hou, L., Peng, H.J., Ding, J., 2015b. Sources of the ore-forming materials for the Yinachang Fe-Cu-Au-REE deposit, Wuding, Yunnan Province: constraints from the ore geology and the S, Pb, H, O isotope geochemistry. J. Asian Earth Sci. 103, 129–149.

Hu, H., Lentz, D., Li, J.W., McCarron, T., Zhao, X.F., Hall, D., 2015. Reequilibration processes in magnetite from iron skarn deposits. Econ. Geol. 110, 1–8.

Hu, H., Duan, Z., Luo, Y., Li, J.W., 2014. Trace element systematics of magnetite from the Chengchao iron deposit in the Daye district: a laser ablation ICP-MS study and insights into ore genesis. Acta Petrol. Sin. 30 (5), 1292–1306.

Ilton, E.S., Eugster, H.P., 1989. Base metal exchange between magnetite and chloride-rich hydrothermal fluid. Geochim. Cosmochim. Acta 53, 291–301.

Jedwab, J., Blanc, G., Boulegue, J., 1989. Vanadiferous minerals from the Nereus Deep, Red Sea. Terra Nova 1, 188–194. https://doi.org/10.1111/j.1365-3121.1989.tb00351.x.

Knipping, J.L., Bilenker, L.D., Simon, A.C., Reich, M., Barra, F., Deditius, A.P., Lundstrom, C., Bindeman, I., Munizaga, R., 2015a. Giant Kiruna-type deposits form by efficient flotation of magmatic magnetite suspensions. Geology. https://doi.org/10.1130/G36650.1.

Knipping, J.L., Bilenker, L.D., Simon, A.C., Reich, M., Barra, F., Deditius, A.P., Wälle, M., Heinrich, C.A., Holtz, F., Munizaga, R., 2015b. Trace elements in magnetite from massive iron oxide-apatite deposits indicate a combined formation by igneous and magmatic-hydrothermal processes. Geochim. Cosmochim. Acta 171, 15–38.

Kou, C.H., Zhang, Z.C., Santosh, M., Huang, H., Zhu, J., 2017. Oldest volcanic-hosted submarine iron ores in South China: Evidence from zircon U-Pb geochronology and geochemistry of the Paleoproterozoic Dahongshan iron deposit. Gondwana Res. 49, 182–204.

Li, X.C., Zhou, M.F., 2015. Multiple stages of hydrothermal REE remobilization recorded in fluorapatite in the Paleoproterozoic Yinachang Fe-Cu-(REE) deposit, Southwest China. Geochim. Cosmochim. Acta 166, 53–73.

Li, X.H., Li, Z.X., Sinclair, J.A., Li, W.X., Carter, G., 2006. Revisiting the “Yanbian Terrane”: implications for Neoproterozoic tectonic evolution of the western Yangtze Block, South China. Precambr. Res. 151, 14–30.

Li, Z.Q., Wang, J.Z., Liu, J.J., Li, C.Y., Du, A.D., Liu, Y.P., Ye, L., 2003. Re-Os dating of molybdenite from Lala Fe-oxide-Cu-Au-Mo-REE deposit, southwest China: implications for ore genesis. Contrib. Geol. & Min. Resour. Res. 18, 39–42 (in Chinese with English abstract).

Liang, H.Y., Sun, W.D., Su, W.C., Zartman, E.R., 2009. Porphyry copper-gold mineralization at Yulong, China, promoted by decreasing redox potential during magnetite alteration. Econ. Geol. 104, 587–596.

Liu, P.P., Zhou, M.F., Chen, W.T., Gao, J.F., Huang, X.W., 2015. In-situ LA-ICP-MS trace elemental analyses of magnetite: Fe–Ti–(V) oxide-bearing mafic–ultramafic layered intrusions of the Emeishan Large Igneous Province, SW China. Ore Geol. Rev. 65, 853–871.

Liu, Y.S., Hu, Z.C., Gao, S., Gunther, D., Xu, J., Gao, C.G., Chen, H.H., 2008. In situ analysis of major and trace elements of anhydrous minerals by LA-ICP-MS without applying an internal standard. Chem. Geol. 257, 34–43.

N9GBYBGMR (No. 9 Geological Brigade of the Yunnan Bureau of Geology and Mineral Resources), 1983. Report of exploration and prospecting of the Dahongshan iron and copper deposits, Xinping County, Yunnan Province: Unpublished report, prepared for Chinese government, 377 p. (in Chinese).

Nadoll, P., Angerer, T., Mauk, J.L., French, D., Walshe, J., 2014. The chemistry of hydrothermal magnetite: a review. Ore Geol. Rev. 61, 1–32.

Nadoll, P., Mauk, J.L., Leveille, R.A., Koenig, A.E., 2015. Geochemistry of magnetite from porphyry Cu and skarn deposits in the southwestern United States. Miner. Deposita 50, 493–515.

Neilson, R., 2003. Trace element partitioning, http://earthref.org/GERM/tolls/tep.htm.

Planavsky, N., Bekker, A., Rouxel, O.J., Kamber, B., Hofmann, A., Knudsen, A., Lyons, T.W., 2010. Rare Earth Element and yttrium compositions of Archean and Paleoproterozoic Fe formations revisited: new perspectives on the significance and mechanisms of deposition. Geochim. Cosmochim. Acta 74, 6387–6405.

Qi, L., Grégoire, D.C., 2000. Determination of trace elements in twenty-six Chinese geochemistry reference materials by inductively coupled plasma mass spectrometry. Geostand. Newslett. 24, 51–63.

Qian, J., Shen, Y., 1990. The Dahongshan volcanogenic Fe-Cu deposit in Yunnan Province: series of geological memoirs of People’s Republic of China. Geological Publishing House, Beijing, p 236 (in Chinese with English abstract).

Rudnick, R., Gao, S., 2003. Composition of the continental crust. Treatise Geochem. 3, 1–64.

Rusk, B., Oliver, N., Cleverley, J., Blenkinsop, T., Zhang, D., Williams, P., Habermann, P., 2010. Physical and chemical characteristics of the Ernest Henry iron oxide copper gold deposit, Australia: implications for IOGC genesis. In: Porter T (ed) Hydrothermal iron oxide copper gold and related deposits: a global perspective, v 3-advances in the understanding of IOCG deposits. PGC Publishing, Adelaide, pp 201–218.

Sun, K., Shen, Y., Liu, G., Li, Z., Pan, X., 1991. Proterozoic iron-copper deposits in central Yunnan Province. China University of Geoscience Press, Wuhan, p 169 (in Chinese with English abstract).

Sun, Z.M., Yin, F.G., Guan, J.L., Liu, J.H., Li, J.M., Geng, Y.R., Wang, L.Q., 2009. SHRIMP U-Pb dating and its stratigraphic significance of tuff zircons from Heishan Formation of Kunyang Group, Dongchuan area, Yunnan Province, China. Geol. Bull. China 28, 896–900 (in Chinese with English abstract).

Toplis, M.L., Corgne, A., 2002. An experimental study of element partitioning between magnetite, clinopyroxene and iron-bearing silicate liquids with particular emphasis on vanadium. Contrib. Mineral. Petrol. 144, 22–37.

Wang, Y.J., Zhu, W.G., Huang, H.Q., Zhong, H., Bai, Z.J., Fan, H.P., Yang, Y.J., 2019. Ca. 1.04 Ga hot Grenville granites in the western Yangtze block, Southwest China. Precambr. Res. 328, 217–234.

Wang, W., Zhou, M.F., 2014. Provenance and tectonic setting of the Paleo to Mesoproterozoic Dongchuan Group in the southwestern Yangtze Block, South China: implication for the breakup of the supercontinent Columbia. Tectonophysics 610, 110–127.
Williams, P.J., Hedenquist, J.W., Barton, M.D., Johnson, D.A., Fontbote, L., de Haller, A., Mark, G., Oliver, N.H.S., Marschik, R., Thompson, J.F.H., Goldfarb, R.J., Richards, J.P., 2005. Iron oxide copper-gold deposits: geology, space-time distribution, and possible modes of origin. Econ. Geol. 100, 371–405.
Wu, K.W., Zhong, H., Zhu, W.G., Leng, C.B., Gou, T.Z., 2008. Study on ore-forming fluid of the Dahongshan stratiform copper deposit, Yunnan, China. Acta Petrol. Sin. 24, 2045–2057 (in Chinese with English abstract).
Yang, H., Liu, F.L., Du, L.L., Liu, P.H., Wang, F., 2012. Zircon U-Pb dating for meta-volcanites in the Laochanghe Formation of the Dahongshan Group in southwestern Yangtze block, and its geological significance. Acta Petrol. Sin. 28, 2994–3014.
Yang, Y.M., Tu, G.Z., Hu, R.Z., 2004. REE geochemistry of Yinachang Fe-Cu-REE deposit in Yunnan province. Acta Geochem. 23 (3), 265–274 (in Chinese with English abstract).
Ye, X.T., Zhu, W.G., Zhong, H., He, D.F., Ren, T., Bai, Z.J., Fan, H.P., Hu, W.J., 2013. Zircon U-Pb and chalcopyrite Re-Os geochronology, REE geochemistry of the Yinachang Fe-Cu-REE deposit in Yunnan Province and its geological significance. Acta Petrol. Sin. 29 (4), 1167–1186 (in Chinese with English abstract).
Zhang, C.H., Gao, L.Z., Wu, Z.J., Shi, X.Y., Yan, Q.R., Li, D.J., 2007. SHRIMP U-Pb zircon age of tuff from the Kunyang group in central Yunnan: evidence for Grenvillian orogeny in south China. Chin. Sci. Bull. 52, 1517–1525.
Zhang, Z.C., Hou, T., Li, H.M., Li, J.W., Zhang, Z.H., Song, X.Y., 2014a. Enrichment mechanism of iron in magmatic hydrothermal system. Acta Petrol. Sin. 30 (5), 1189–1204 (in Chinese with English abstract).
Zhang, Z.C., Hou, T., Santosh, M., Li, H.M., Li, J.W., Zhang, Z.H., Song, X.Y., Wang, M., 2014b. Spatio-temporal distribution and tectonic settings of the major iron deposits in China: an overview. Ore Geol. Rev. 57, 247–263.
Zhao, X.F., Zhou, M.F., 2011. Fe-Cu deposits in the Kangdian region, SW China: a Proterozoic IOCG (iron-oxide-copper-gold) metallogenic province. Miner. Deposita 46, 731–747.
Zhao, X.F., Zhou, M.F., Li, J.W., Seley, D., Li, X.H., Qi, L., 2013. Sulfide Re-Os and Rb-Sr isotope dating of the Kangdian IOCG metallogenic province, southwest China: implications for regional metallogenesis. Econ. Geol. 108, 1489–1498.
Zhao, X.F., Zhou, M.F., Li, J.W., Sun, M., Gao, J.F., Sun, W.H., Yang, J.H., 2010. Late Paleoproterozoic to early Mesoproterozoic Dongchuan Group in Yunnan, SW China: implications for tectonic evolution of the Yangtze Block. Precambr. Res. 182, 57–69.
Zhao, X.F., Zhou, M.F., Su, Z.K., Li, X.C., Chen, W.T., Li, J.W., 2017. Geology, geochronology, and geochemistry of the Dahongshan Fe-Cu-(Au-Ag) deposit, Southwest China: implications for the formation of Iron Oxide Copper-Gold Deposits in intracratonic rift settings. Econ. Geol. 112, 603–628.
Zhou, M.F., Ma, Y., Yan, D.P., Xia, X., Zhao, J.H., Sun, M., 2006. The Yanbian Terrane (Southern Sichuan Province, SW China): a Neoproterozoic arc assemblage in the western margin of the Yangtze Block. Precambr. Res. 144, 19–38.
Zhou, M.F., Zhao, X.F., Chen, W.T., Li, X.C., Wang, W., Yan, D.P., Qiu, H.N., 2014. Proterozoic Fe-Cu metallogeny and supercontinental cycles of the southwestern Yangtze Block, southern China and northern Vietnam. Earth Sci. Rev. 139, 59–82.
Zhou, Z.J., Tang, H.S., Chen, Y.J., Chen, Z.L., 2017. Trace elements of magnetite and iron isotopes of the Zankan iron deposit, westernmost Kunlun, China: a case study of seafloor hydrothermal iron deposits. Ore Geol. Rev. 80, 1191–1205.
Zhu, W.G., Zhong, H., Li, Z.X., Bai, Z.J., Yang, Y.J., 2016. SIMS zircon U-Pb ages, geochemistry and Nd-Hf isotopes of ca. 1.0 Ga mafic dykes and volcanic rocks in the Huili area, SW China: Origin and tectonic significance. Precambr. Res. 273, 67–89.
Zhu, Z.M., Tan, H.Q., Liu, Y.D., Li, C., 2017. Multiple episodes of mineralization revealed by Re-Os molybdenite geochronology in the Lala Fe-Cu deposit, SW China. Miner. Deposita DOI:10.1007/s00126-017-0740-x.